Appendix

Index:

Statistical Methods

- **Weighted-max peak: page 2**
- **Linear regression model of CAG repeats versus the ratio of UHDRS-TMS at baseline and age at onset: page 3**
  Hierarchical clustering: page 4

Brain Imaging

- **Retrospective Magnetic Resonance Imaging (MRI) and MRI single voxel proton spectroscopy (MRS) analysis: page 5**

Brain imaging atlas: page 6eTables

- **eTable 1: page 7**
- **eTable 2: page 8**
- **eTable 3: page 9**
- **eTable 4: page 10**
- **eTable 5: page 11**
- **eTable 6: page 13**
- **eTable 7: page 14**
- **eTable 8: page 15**
- **eTable 9: page 16**

eFigures Legends

- **eFigure 1: page 17**
- **eFigure 2: page 17**
- **eFigure 3: page 17**
- **eFigure 4: page 17**
- **eFigure 5: page 17**
- **eFigure 6: page 17**
- **eFigure 7: page 18**

eFigures

- **eFigure 1: page 19**
- **eFigure 2: page 20**
- **eFigure 3: page 21**
- **eFigure 4: page 22**
- **eFigure 5: page 23**
- **eFigure 6: page 24**
- **eFigure 7: page 25**

Weighted-max peak method

In order to obtain a measure of mosaicism, we took inspiration from the Instability Index proposed by Lee et al. (2010).[11] We obtained PCR amplification of trinucleotide repeats viewed using GeneMapper software as a cluster of peaks (J) differing by a single CAG repeat. For each patient, we identified the maximum of the peak heights (ph) among the cluster of peaks J:

$$M_{ph} = \max_{j \in J} ph_j$$

From M_{ph}, we computed the relative threshold for the background correction as the 20% of M_{ph} and considered only those peaks with height higher than this threshold. Hence, we worked with a new cluster of peaks P, that is a subset of J.

We then counted the number of peaks that are located on the right side of M_{ph}:

$$n_P = \sum_{j \in P} i_j$$

where $i_j$is the indicator variable that is set to one if the peak position is at the right of the position m of M_{ph}:

$$i_j = \begin{cases} 0, & j < m \\ 1, & j > m \end{cases}$$

The proportion of peaks located at the right side of M_{ph}, can be written as the ratio of n_P and the total number of peaks (N) belonging to the subset P:

$$w = \frac{n_P}{N}$$

Because of its positive sign, this measure takes into account only the expansion of the peaks and not the contraction. To better define the contraction of the peaks, we reverted the sign of w if its value was less to 0·5:

$$w = \begin{cases} -w, & if\ w < 0 \cdot 5 \\ 0, & if\ w = 0 \cdot 5 \\ w, & if\ w > 0 \cdot 5 \end{cases}$$

$w > 0 \cdot 5$ means that the majority of peaks are on the right side of m and that, if $w < 0 \cdot 5$, the peaks are contracted. The value of $w = 0 \cdot 5$ indicates a balanced peaks distribution, hence the subject can be considered as *neutral* by setting the weight equal to zero. The measure w can be seen as a weight of the maximum peak M_{ph}.

In this way, for a single patient, we can construct the *weighted-max peak index* as the product of w and M_{ph}:

$$W_{mp} = w \cdot M_{ph}$$

This index will be negative if the peaks are contracted and it will be positive if the peaks are expanded and it can be seen as a measure of the CAG expansion instability.

Linear regression model of CAG repeats versus the ratio of UHDRS-TMS at baseline and age at onset

In order to study the linear dependence between CAG, UHDRS-TMS and age at onset in JHD cohort, we took inspiration from Penney et al. (1997)[17], that have estimated the striatal dysfunction by a linear regression model between CAG and the quotient of striatal pathology divided by age (equation 1 of [17]). Instead of the striatal pathology, we considered the only validated tool to measure HD motor impairment, which is the UHDRS-TMS, and performed a linear regression model between the CAG and the ratio of UHDRS-TMS at baseline and the age at onset. The resulting regression model is shown below.

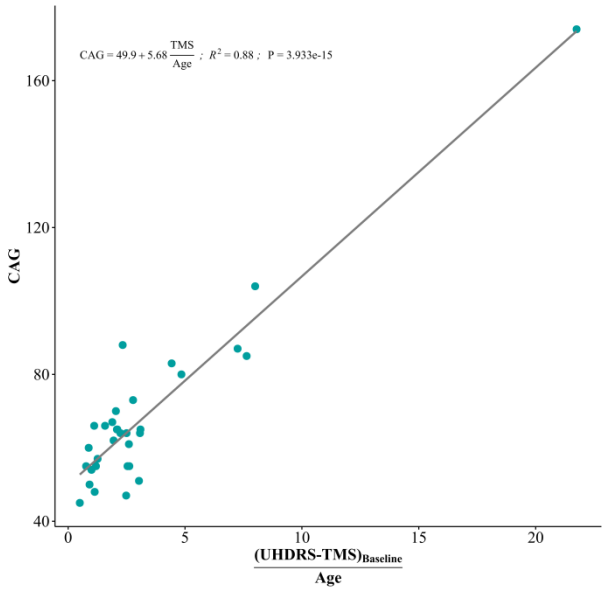

For the longitudinal analysis, we used the UHDRS -TMS measure and, for CAP computations at baseline, we considered the age of the patient at the time of baseline of UHDRS-TMS measurement. We have modelled the observed UHDRS -TMS by using a GEE approach, where several different model specifications have been considered; first, we have used different scales for the response, in order to improve approximate normality. Second, we have considered different working covariance matrices to be used to get estimates within the GEE approach. In all cases, the conclusions were qualitatively similar to those obtained by using the linear scale and the exchangeable correlation structure.

The QQplot of model residuals would indicate that the small sample size and number of occasions for each individual might lead to some bias in parameter estimates, as the observed distribution has heavier tails when compared to the Gaussian distribution. However, even when working with a log transform, which closely approximate residuals to a normal distribution, we obtained the same results. The effect of Time and Time*Category (eTable 7) on UHDRS -TMS were significant anyways. Finally, we adopted the BCgee approach suggested by Lundaron and Scharfstein (2017) to face the bias of the GEE estimates that may be caused by the limited sample size. Even in this case, we obtained very similar results. Hence, all these facts made us sufficiently confident to make conclusions from these results.

Hierarchical clustering

Hierarchical clustering is a method of cluster analysis that consists in grouping similar objects. In our case, we would like to discover groups (or clusters) of patients inside the Juvenile Huntington disease cohort. The application of such method refers to the variables of the regression model discussed in the previous section: CAG and the ratio between the UHDRS-TMS and age.

There are two main strategies for discovering clusters:

- a bottom-up strategy (or agglomerative), which starts with a number of clusters equal to the number of observations (i.e. each cluster is composed by a single observation) and, then, similar observations are joined until a unique cluster, with all patients belonging to it, is reached;
- a top-down approach (or divisive), which starts with one cluster composed of all observations and, through a successive splitting, ends when each cluster has one observation.

The basic idea in both strategies consists of joining or splitting observations on the basis of a similarity measure. In our application, as similarity measure, we used the Euclidean distance between pairs of observations:

$$d(a,b) = \|a - b\|_2 = \sqrt{\sum_i (a_i - b_i)^2}$$

where a and b are two different observations.

The optimal result of the clustering is to find the best partition of the observations such that groups are well separated and each group has high within-cohesion. Hence, each group is constructed such that the distance between observations in a group is low and the distance between cluster is high. The latter is measured through a linkage criterion that is a function of the pairwise Euclidean distances observations in the sets. For this purpose, we have chosen the average linkage method:

$$\frac{1}{|A||B|}\sum_{a\in A}\sum_{b\in B} d(a,b)$$

where A and B are two sets of observations.

The clustering operations attempt to represent all similarity judgements accurately in terms of standard similarity structures such as a dendrogram (or tree). In this representation, the height of each node in the plot is proportional to the value of the intergroup dissimilarity between its two merger clusters (the bottom nodes representing individual observations are all plotted at zero height).

Retrospective magnetic resonance imaging (MRI) and MRI single voxel proton spectroscopy (MRS) analysis

Patients who performed MRI scan (n=4) had infantile motor abnormalities and a mutation size beyond 80 CAG repeats (IQR 4). MRS scans of both striatal nuclei were available for two children. Because patients were located in different regions, MRI scans were not performed in the same machine, but all images were generated from a 1.5 Tesla MRI scanner with T1- and T2-weighted, fluid-attenuated inversion recovery (FLAIR) and diffusion-weighted imaging sequences, and compared with images of normal children in the identical range of ages.[1] All MRI and MRS scans were re-analysed by a neuroradiologist with expertise in HD. Rare *post mortem* pathological brain images from a single case of infantile HD were also examined (provided by the New York Brain Bank, Columbia University, New York, NY, USA). In all four children, MRI and MRS brain imaging revealed an early, selective and bilateral pathological involvement of both striatal nuclei (eFigure 3), but no significant cortical or white matter involvement and reduced neuronal density and membrane markers (eFigure 4-7). In particular, the volume of the striatal nuclei (i.e. caudate nucleus and putamen) was remarkably and globally reduced. The *post mortem* brain sample at a final neuropathological degree 4, obtained from a fifth child, who had died aged 8 years, carrying a large sized mutation of 82 CAG repeats, at an advanced HD stage, confirmed the imaging (eFigure 3).

MRS imaging highlighted the striatal neuronal damage, with decreases in neural density and neuronal membrane markers, as indicated by reduced *N*-acetyl-aspartate (NAA):creatine (Cr) and choline(Cho):Cr ratios (eFigure 5). These ratios were lower in child OM-HD01, who carried a particularly large mutation (NAA:Cr ratio=1·10, Cho:Cr ratio=0·95; age at onset 1·5 years; 174 CAG repeats) than child HD636 (NAA:Cr ratio=2·79, Cho:Cr ratio=1·58; age at onset 3; 84 CAG repeats) (eFigure 5). By contrast, all other brain structures in these and the other children appeared normal (eFigure 3-7). Indeed, cerebral cortex thickness and sulci distribution were normal, there were no white matter focal changes in signal intensity, and the morphology and thickness of the corpus callosum were also normal (eFigure 3-7). Moreover, there were no additional abnormal focal areas of altered signal intensity in the brainstem and cerebellum. Taken together, MRI and MRS and brain pathology signs suggested an early, selective and bilateral pathological involvement of both striatal nuclei.

1. Fonov V, Evans AC, Botteron K, Almli CR, McKinstry RC, Collins DL. Unbiased average age-appropriate atlases for pediatric studies. *NeuroImage* 2011; **54:** 313–27.

Brain imaging atlas

MRI brain atlas especially was devoted to the pediatric brain studies,[16] in order to avoid the inter- and intra-individual variability of brain morphology, and to provide more accurate and normative data. Furthermore, this pediatric brain atlas was generated from the largest epidemiological, representative (healthy and normal) sample of United States pediatric population (433 healthy subjects), from 6 sites, where each subject was carefully screened for medical and psychiatric factors. Moreover, in this atlas, brain images were acquired by MRI 1.5 Tesla scans, similarly to the scans shown in our study. We used this brain atlas image for illustrative purpose only, in eFigure 1, in comparison with the MRI brain JHD.

eTable 1. Demographics and clinical characteristics of patients who underwent MRI.

Patient code	Centre	Gender	Expanded CAG repeat number	Age at onset, years	Initial motor phenotype	Time between age at onset and MRI, years	UHDRS -TMS at MRI/MRS
OM-HD01	Oman	M	174	1·5	Dystonia	5·5	103
HD636	Italy	F	84	3	Parkinsonism or dystonia	5	31
HD305	Italy	M	80	6	Dystonia	7	63
HD178	Italy	F	88	6	Parkinsonism	8	48

F, female; M, male; MRI, Magnetic Resonance Imaging; MRS, MRI single voxel proton spectroscopy; NA, not applicable; UHDRS−TMS, Huntington Disease Rating Scale–Total Motor Score.

eTable 2. Motor symptoms of patients with JHD, as described by patients' caregivers.

Motor symptoms	HE (n=10)	LE (n=26)	Total (N=36)	p-value
Gait disorder				
No	2 (20%)	19 (73·08%)	21 (58·4%)	**0·0071**
Yes	8 (80%)	7 (26·92%)	15 (41·6%)	
Oral motor impairment				
No	4 (40%)	24 (92·31%)	28 (77·7%)	**0·0024**
Yes	6 (60%)	2 (7·69%)	8 (22·3%)	
Orofacial tics				
No	9 (90%)	20 (76·92%)	29 (80·5%)	0·6454
Yes	1 (10%)	6 (23·08%)	7 (19·5%)	
Clumsiness				
No	10 (100%)	15 (57·69%)	25 (69·5%)	**0·0160**
Yes	0 (0%)	11 (42·31%)	11 (30·5%)	
Involuntary movements				
No	9 (90%)	20 (76·92%)	29 (77·7%)	0·6454
Yes	1 (10%)	6 (23·08%)	7 (19·3%)	

Data are n (%). Values in bold denote statistical significance (Fisher's exact test, $p<0·05$) for the comparison of presence of symptoms (HE vs LE).

HE, highly expanded; JHD, juvenile Huntington's disease; LE, low expansion.

'No' is used when a given symptom is absent.

eTable 3. Main motor onset phenotype of patients with JHD, as reported in patients' medical records.

Motor phenotype	HE (n=10)	LE (n=26)	Total (N=36)	p-value
Chorea	0 (0%)	6 (23·08%)	6 (16·7%)	0·052
Dystonia and parkinsonism	9 (90%)	17 (65·4%)	26 (72·2%)	
Incoordination	1 (10%)	1 (3·85%)	2 (5·6%)	
Tics	0 (0%)	2 (7·69%)	2 (5·6%)	

Data are n (%). Values in bold denote statistical significance (Chi-Squared test, $p<0·05$) for the comparison of the presence of symptoms (HE vs LE).

HE, highly expanded; JHD, juvenile Huntington's disease; LE, low expansion.

eTable 4. Predominant motor manifestations of JHD, as reported in patients' medical records during the disease course.

Motor symptoms	HE (n=10)	LE (n=26)	Total (N=36)	p-value
Severe dysarthria or dysphagia				
No	2 (20%)	12 (46·15%)	14 (38·9%)	0·2545
Yes	8 (80%)	14 (53·85%)	22 (61·1%)	
Severe gait impairment				
No	1 (10%)	17 (65·38%)	18 (50·0%)	**0·0072**
Yes	9 (90%)	9 (34·62%)	18 (50·0%)	
Bradykinesia				
No	6 (60%)	8 (30·77%)	14 (38·9%)	0·1401
Yes	4 (40%)	18 (69·23%)	22 (61·1%)	
Rigidity				
No	3 (30%)	10 (38·46%)	13 (36·1%)	0·7160
Yes	7 (70%)	16 (61·54%)	23 (63·9%)	
Dystonia				
No	0 (0%)	7 (26·92%)	7 (19·5%)	0·1547
Yes	10 (100%)	19 (73·08%)	29 (80·5%)	
Chorea				
No	10 (100%)	17 (65·38%)	27 (75%)	**0·0394**
Yes	0 (0%)	9 (34·62%)	9 (25%)	
Tics				
No	8 (80%)	17 (65·38%)	25 (69·5%)	0·6880
Yes	2 (20%)	9 (34·62%)	11 (30·5%)	
Ataxia				
No	9 (90%)	23 (88·46%)	32 (88·9 %)	1
Yes	1 (10%)	3 (11·54%)	4 (11·1%)	
Tremor				
No	9 (90%)	18 (69·23%)	27 (75·0%)	0·3921
Yes	1 (10%)	8 (30·77%)	9 (25·0%)	
Myoclonus				
No	9 (90%)	22 (84·62%)	31 (86·1%)	1
Yes	1 (10%)	4 (15·38%)	5 (13·9%)	

Data are n (%). Values in bold denote statistical significance (Fisher's exact test, $p<0·05$) for the comparison of the presence of symptoms (HE vs LE). HE, highly expanded; JHD, juvenile Huntington's disease; LE, low expansion. 'No' is used when a given symptom is absent.

eTable 5. Non-motor manifestations of JHD, as reported in patients' medical records during the disease course.

Non-motor symptoms	HE (n=10)	LE (n=26)	Total (N=36)	p-value
Development delay				
No	1 (10%)	26 (100%)	27 (75·0%)	**<0·0001**
Yes	9 (90%)	0 (0%)	9 (25·0%)	
Learning failure				
No	7 (70%)	21 (80·77%)	28 (77·8%)	0·6576
Yes	3 (30%)	5 (19·23%)	8 (22·2%)	
Cognitive decline				
No	9 (90%)	18 (69·23%)	27 (75·0%)	0·3921
Yes	1 (10%)	8 (30·77%)	9 (5·0%)	
Obsessive behaviour				
No	8 (80%)	7 (26·92%)	15 (41·7%)	**0·0071**
Yes	2 (20%)	19 (73·08%)	21 (58·3%)	
Compulsive behaviour				
No	8 (80%)	21 (80·77%)	29 (80·5%)	1
Yes	2 (20%)	5 (19·23%)	7 (19·5%)	
Psychosis				
No	10 (100%)	20 (76·92%)	30 (83·3%)	0·1567
Yes	0 (0%)	6 (23·08%)	6 (16·7%)	
Autistic behaviour				
No	8 (80%)	25 (96·15%)	33 (91 ·7%)	0·1807
Yes	2 (20%)	1 (3·85%)	3 (8·3%)	
Mood changes				
No	9 (90%)	14 (53·85%)	23 (63·9%)	0·0596
Yes	1 (10%)	12 (46·15%)	13 (36·1%)	
Personality changes				
No	10 (100%)	22 (84·62%)	32 (88·9%)	0·5586
Yes	0 (0%)	4 (15·38%)	4 (11·1%)	
Irritability or aggressiveness				
No	8 (80%)	16 (61·54%)	24 (66·7%)	0·4383
Yes	2 (20%)	10 (38·46%)	12 (33·3%)	
Perseverations				
No	10 (100%)	13 (50%)	23 (63·9%)	**0·0058**
Yes	0 (0%)	13 (50%)	13 (36·1%)	

Suicidal behaviour				
No	10 (100%)	19 (73·08%)	29 (80·5%)	0·1547
Yes	0 (0%)	7 (26·92%)	7 (19·5%)	

Data are n (%). Values in bold denote statistical significance (Fisher's exact test, $p<0·05$) for the comparison of the presence of symptoms (HE vs LE).

HE, highly expanded; JHD, juvenile Huntington's disease; LE, low expansion.

'No' is used when a given symptom is absent.

eTable 6. Seizures, as reported in patients' medical records during the disease course.

Seizures	HE (n=10)	LE (n=26)	Total (N=36)	p-value
No	2 (20%)	23 (88·46%)	25 (69·5%)	**<0·0001**
Yes	8 (80%)	3 (11·54%)	11 (30·5%)	

Data are n (%). Values in bold denote statistical significance (Fisher's exact test, $p<0·05$) for the comparison of the presence of symptoms (HE vs LE). HE, highly expanded; JHD, juvenile Huntington's disease; LE, low expansion.

'No' is used when a given symptom is absent.

eTable 7. Clinical characteristics of patients included in the survival analysis.

Characteristics	JHD HE	JHD LE	Adult-onset HD	*p*-value
Deceased patients, n	9	8	104	-
Censored patients, n	0	2	93	-
Median (range) number of CAG repeats	88 (80 - 174)	62·5 (54 - 73)	44 (40 - 50)	***<0·0001***
Median (range) age at onset, years	4 (2 - 8)	18 (8 - 20)	44 (30 - 60)	***<0·0001***
Median (range) survival time following the first symptom, years	9 (7 - 14)	17 (9 - 29)	14 (2 - 34)	***0·0154***

Values in bold denote statistical significance (Mann-Whitney U test, $p < 0{\cdot}05$) for the comparison HE vs LE.

Continuous variables are expressed as median and their range (min-max).

HD, Huntington's disease; HE, highly expanded; JHD, juvenile Huntington's disease; LE, low expansion.

eTable 8. Generalized Estimating Equation (GEE) results.

Variable	DF	Chi-Square	P
Category	1	0·2	***0·6337***
Time Point	3	159·3	***<0.0001***
Category*Time Point	3	18·6	***0·0003***

Values in bold denote statistical significance ($p < 0·05$) for the comparison of UHDRS-TMS trends between JHD and AHD. DF, Degrees of Freedom; P, P-value; UHDRS-TMS, Huntington Disease Rating Scale – Total Motor Score; JHD, juvenile Huntington's disease; AHD, Adult-onset HD.

eTable 9. Juvenile Huntington's disease patients according to CAG repeat expansion, age at onset and first neurological manifestations

N	HD Code	Cathegory (by expansion)	CAG expansion (n)	Age at onset (years)	First motor symptoms
1	HD16804	HE	104	2	Incoordination
2	OM-HD0101	HE	174	2	Dystonia
3	HD3903	HE	114	3	Dystonia
4	HD63601	HE	83	3	Dystonia
5	ARG03	HE	80	4	Parkinsonism
6	HD19502	HE	85	4	Dystonia
7	HD37905	HE	87	4	Dystonia
8	HD17804	HE	88	6	Parkinsonism
9	HD30501	HE	80	6	Dystonia
10	HD60 11	HE	84	8	Parkinsonism
11	ARG02	LE	64	8	Parkinsonism
12	HD31501	LE	73	10	Dystonia
13	HD30601	LE	65	11	Incoordination
14	HD42302	LE	51	12	Parkinsonism
15	HD43801	LE	66	12	Chorea
16	HD4705	LE	64	12	Tics
17	HD0505	LE	67	13	Parkinsonism
18	HD20402	LE	65	13	Parkinsonism
19	HD46601	LE	60	15	Dystonia
20	ARG01	LE	66	16	Parkinsonism
21	HD38202	LE	48	16	Chorea
22	HD59401	LE	50	16	Parkinsonism
23	HD8307	LE	62	16	Chorea
24	HD0901	LE	70	17	Parkinsonism
25	HD2402	LE	64	18	Chorea
26	HD4706	LE	55	18	Parkinsonism
27	HD9301	LE	54	18	Parkinsonism
28	HD0908	LE	57	19	Chorea
29	HD4209	LE	47	19	Parkinsonism
30	HD16302	LE	65	20	Tics
31	HD32601	LE	55	20	Dystonia
32	HD46901	LE	55	20	Parkinsonism
33	HD67202	LE	41	20	Parkinsonism
34	HD9307	LE	45	20	Chorea
35	OM-HD0105	LE	55	20	Dystonia
36	OM-HD0112	LE	61	20	Parkinsonism

eFigure Legends:

eFigure 1. Stratification of JHD patients.

Hierarchical clustering results showing the classification of the JHD cohort into three groups (blue, red and green) is reported in panel A. The definition of HE (dots) and LE (squares) groups based on CAG repeats is shown in panel B. Difference in triplet mosaicism between weighted-max peak indices of HE (red dots) and LE (green triangles) groups is shown in panel C (t-test p-value=0·00053). The difference in the number of observations between panel B (n=7) and panel C (n=8) depends on UHDRS–TMS data availability.
JHD, juvenile Huntington's disease; HE, highly expanded; LE, low expansion; UHDRS–TMS, Unified Huntington's Disease Rating Scale Total Motor Score.

eFigure 2. Motor and non-motor manifestations of JHD at disease onset and follow-up.
First clinical manifestations of JHD, as described by patients' caregivers, are shown in A. Main motor onset phenotype of JHD reported in patient records are reported in B. Motor manifestations of JHD reported in medical records during the disease course are shown in C. Non-motor manifestations of JHD reported in medical records during the disease course are reported in D.
*p<0·05, **p<0·01, ***p<0·001 for the comparison of the presence of symptoms, HE vs LE.
JHD, juvenile Huntington's disease.

eFigure 3. Selective damage of striatum and integrity of corpus callosum and hippocampus in two JHD patients.
Fresh brain sections and haematoxylin-eosin stains obtained by brain specimens of the 8-year-old JHD patient (T4501) with 82 CAG repeats (top). Brain MRI images from the 8-year-old JHD patient (HD636) with 84 CAG repeats (bottom). Black and red arrows show the striatum atrophy, the preserved corpus callosum and hippocampus, respectively, in T4501 and HD636 patients.
JHD, juvenile Huntington's disease.

eFigure 4. Normal vs JHD brain
A and C panels: coronal and axial T1-weighted MRI atlas images from healthy children with age included between 4.5 and 8.5 years (Fonov et al., 2011). B and D panels: Coronal and axial T1-weighted MRI images from a 7 years old infant with Huntington disease patient OMHD-01, carrying 174 CAG repeats. The red arrows indicate the atrophy of both caudate and putamen nuclei.
JHD, juvenile Huntington's disease; MRI, magnetic resonance imaging.

eFigure 5. MRS obtained by two JHD subjects.
A panel: a 7-years-old JHD subject with 174 CAG repeats (OM-HD01); B panel: a 8-years-old JHD subject (HD636) with 84 CAG repeats. First subject shows a more remarkable reduction of NAA:Cr and Cho:Cr values (1.10 and 0.95, respectively) compared with the second subject (2.79 and 1.58, respectively).
JHD, juvenile Huntington's disease

eFigure 6. Brain MRI scans from patient HD305.
(A) Axial FLAIR and (B) axial T1-weighted images show loss of volume and focal signal changes (FLAIR hyperintensity) of both striatal nuclei (red arrows). (C) The sagittal T1-weighted image shows normal morphology and thickness of the corpus callosum (red arrow). Cortical thickness and sulcal distribution are unremarkable.

FLAIR, fluid-attenuated inversion recovery; MRI (magnetic resonance imaging.

eFigure 7. Brain MRI scans from patient HD178.

(A) Axial T2-weighted and (B) coronal FLAIR sequences show loss of volume and focal signal changes (T2-weighted and FLAIR hyperintensity) of both striatal nuclei (red arrows). There is a slight dilation of both frontal horns of lateral ventricles due to striatal atrophy (red arrows). (C) The sagittal T1-weighted image shows normal corpus callosum morphology and thickness (red arrow). Cortical thickness and sulcal distribution are unremarkable.

FLAIR (fluid-attenuated inversion recovery); MRI (magnetic resonance imaging).

eFigure 1

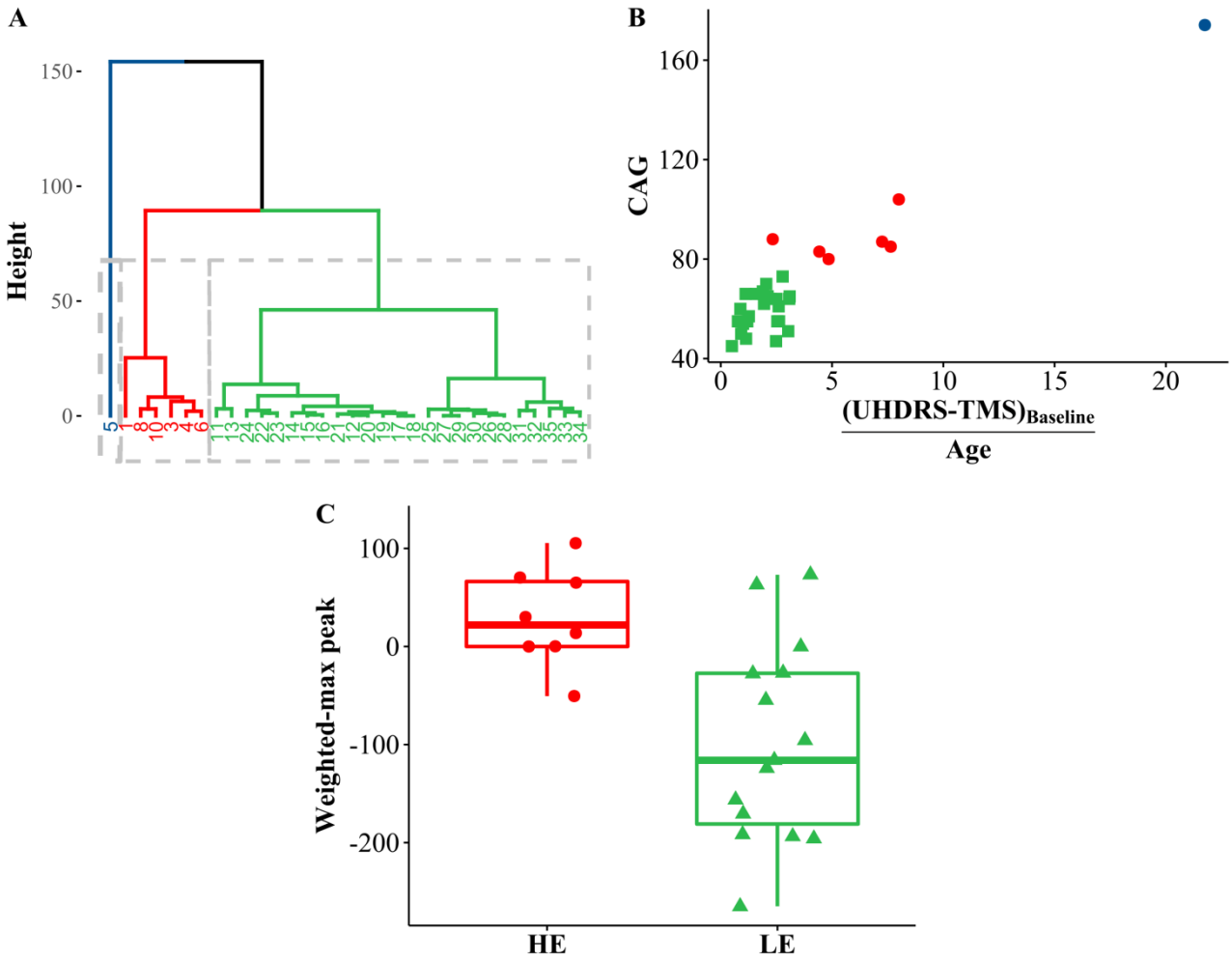
A
Height
150
100
50
0
B
CAG
160
120
80
40
0
5
10
15
20
(UHDRS-TMS)Baseline
Age
C
Weighted-max peak
100
0
-100
-200
HE
LE

eFigure 2

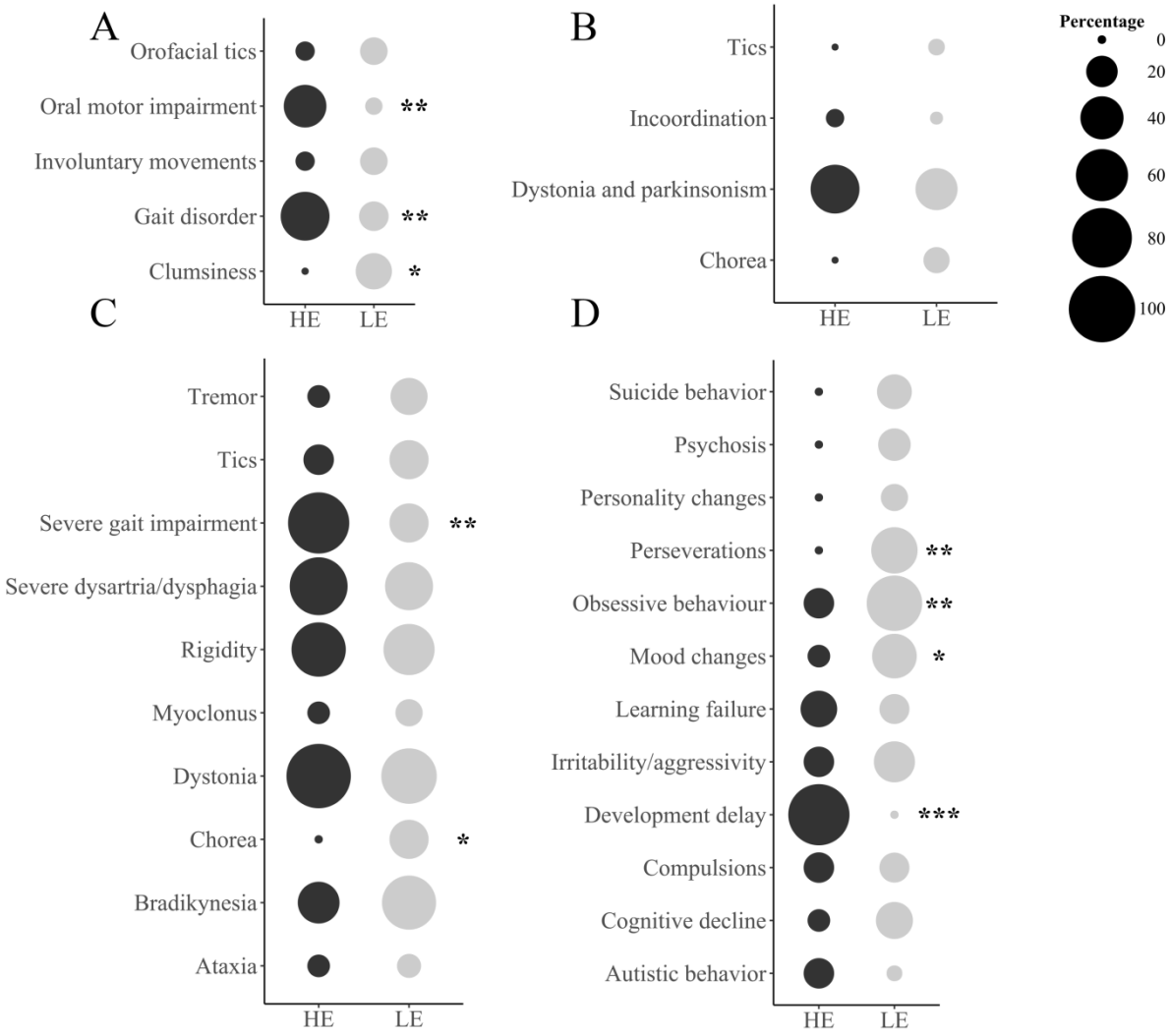
A
Orofacial tics
Oral motor impairment
Involuntary movements
Gait disorder
Clumsiness
**
**
*
HE
LE
B
Tics
Incoordination
Dystonia and parkinsonism
Chorea
HE
LE
Percentage
0
20
40
60
80
100
C
Tremor
Tics
Severe gait impairment
Severe dysartria/dysphagia
Rigidity
Myoclonus
Dystonia
Chorea
Bradikynesia
Ataxia
**
*
HE
LE
D
Suicide behavior
Psychosis
Personality changes
Perseverations
Obsessive behaviour
Mood changes
Learning failure
Irritability/aggressivity
Development delay
Compulsions
Cognitive decline
Autistic behavior
**
**
*
***
HE
LE

eFigure 3

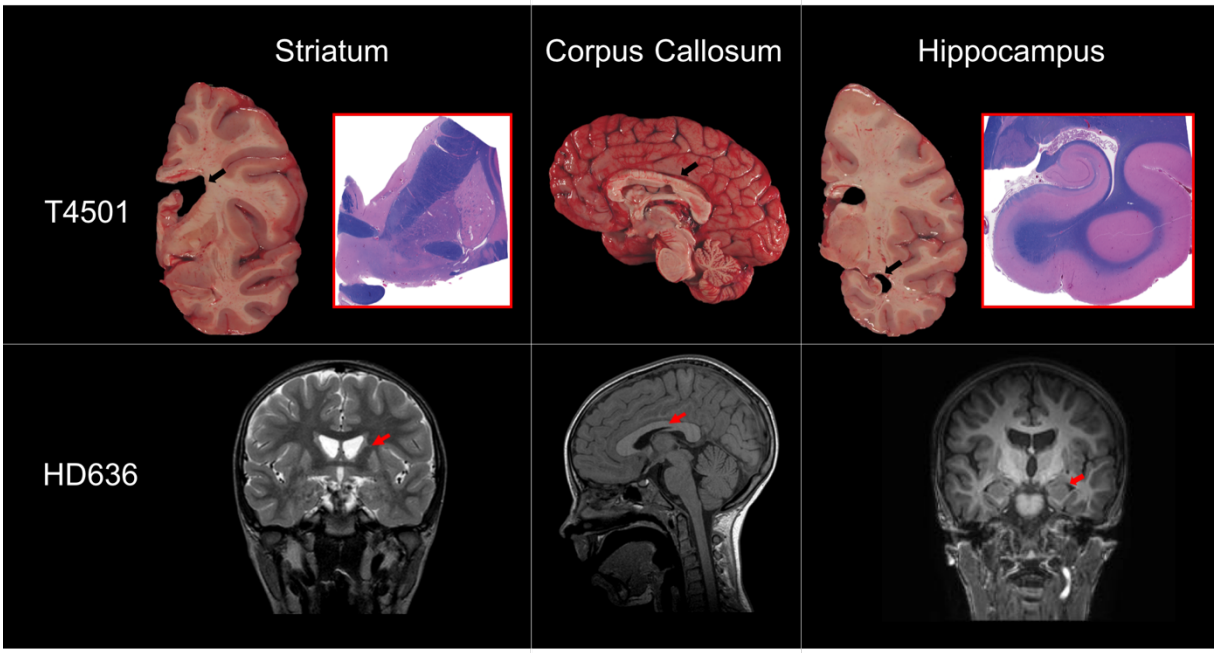

eFigure 4

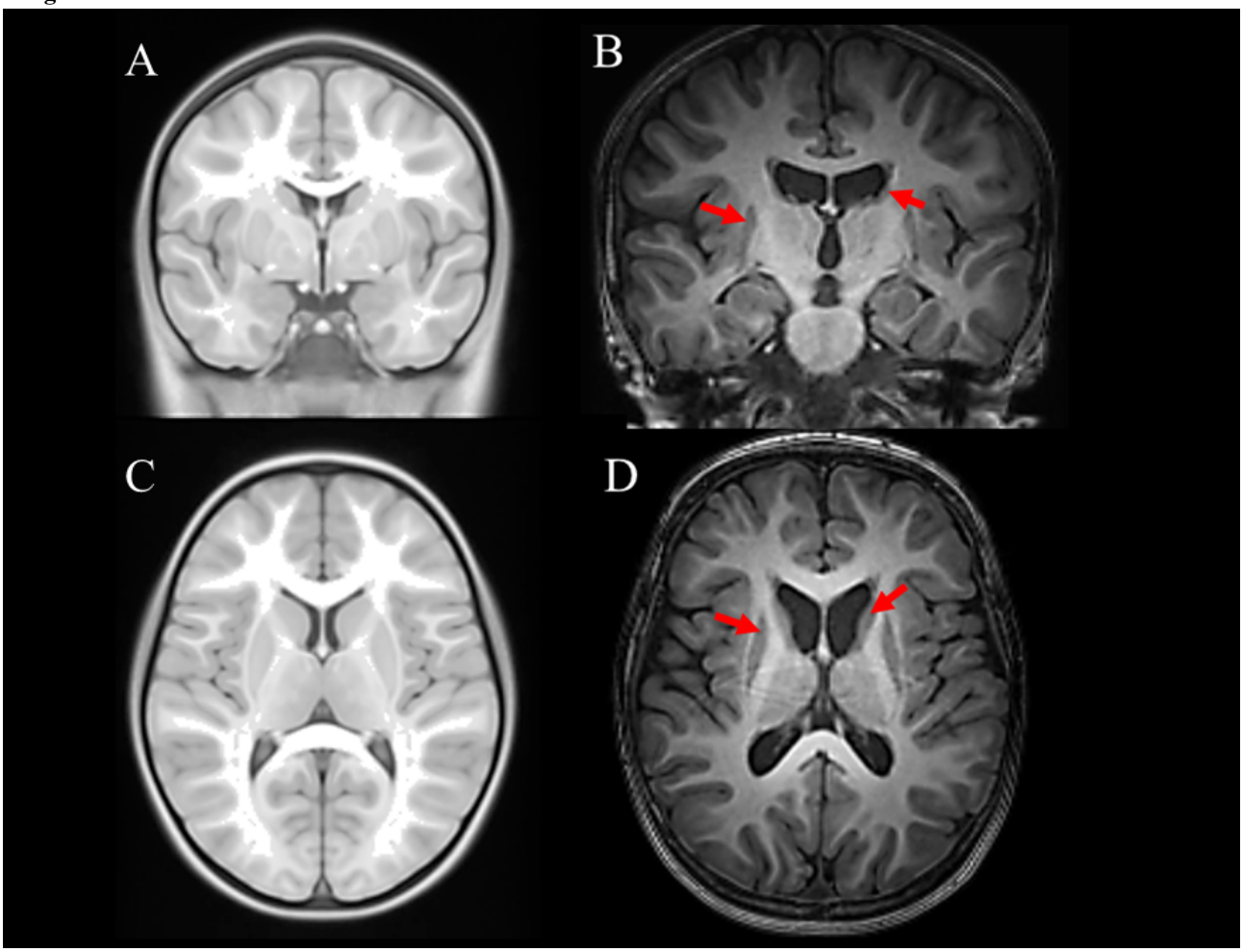

eFigure 5

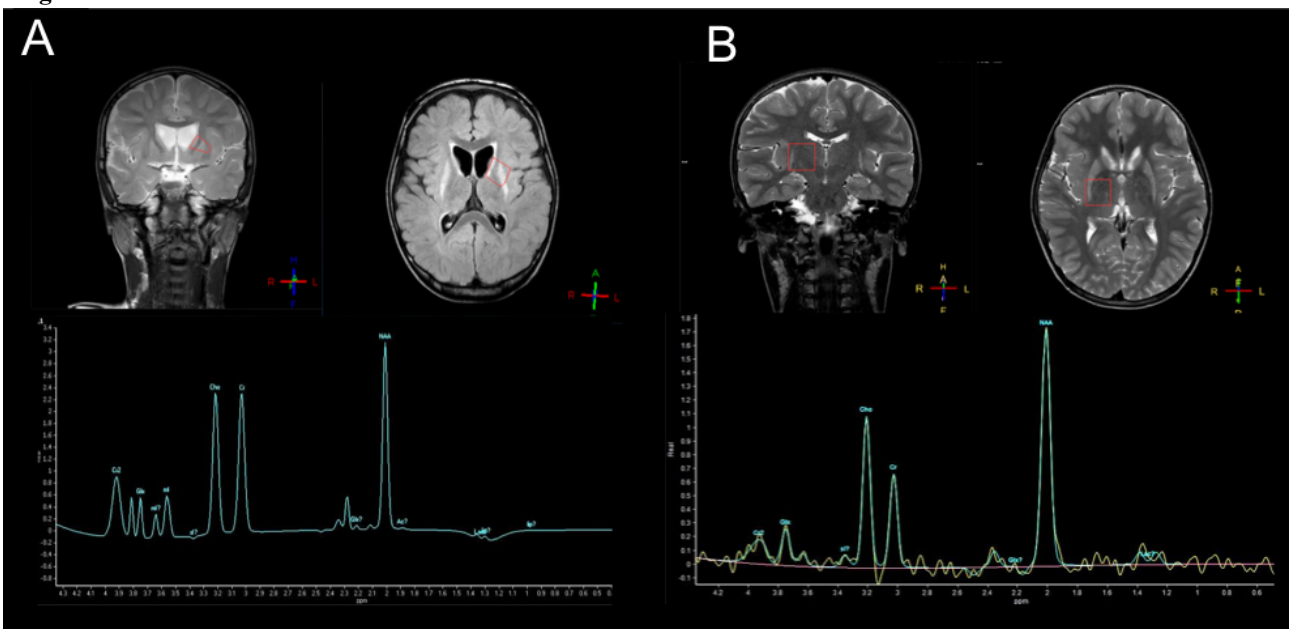

eFigure 6

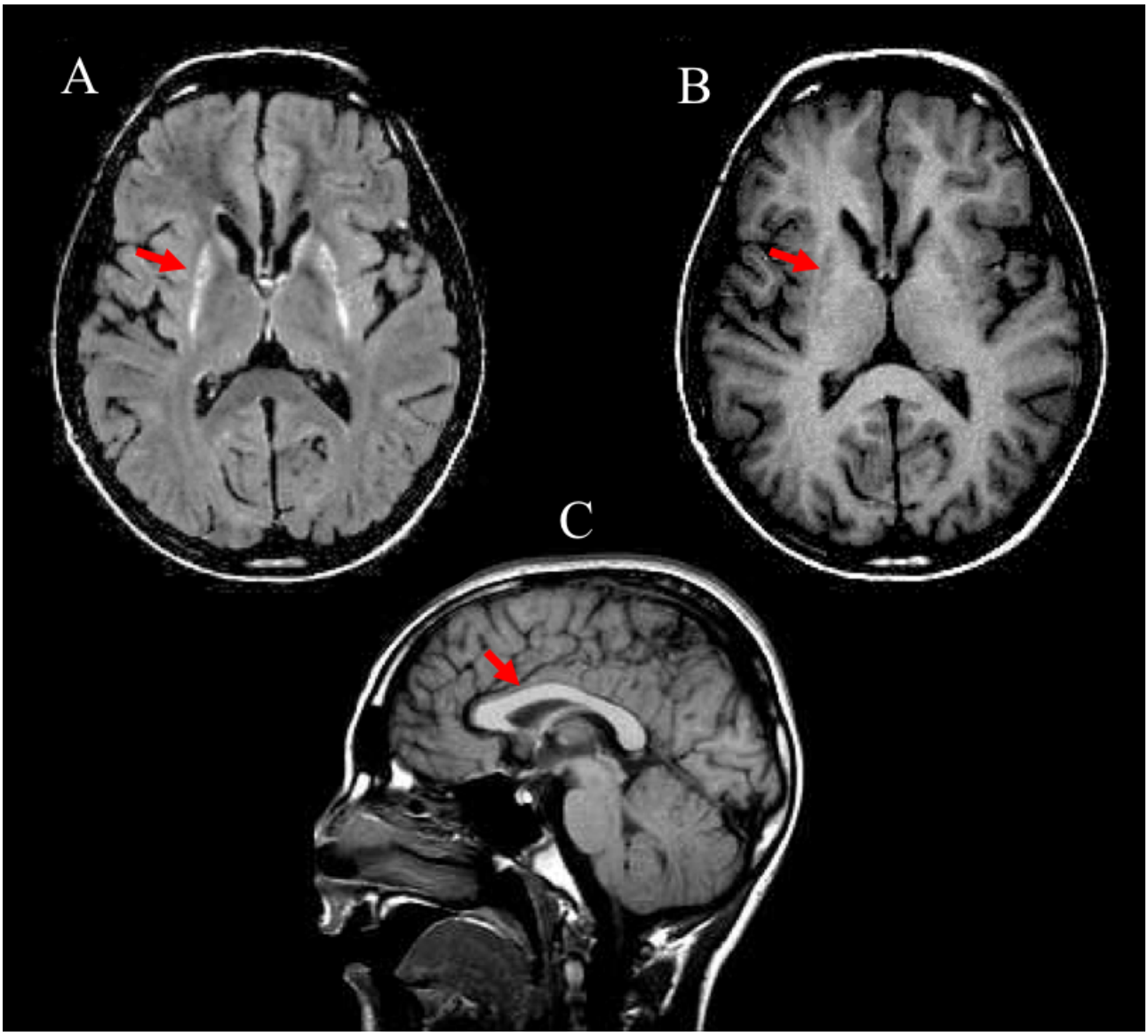

eFigure 7